Sensors

Deutsche Ausgabe: DOI: 10.1002/ange.201708606
Internationale Ausgabe: DOI: 10.1002/anie.201708606

Room-Temperature-Phosphorescence-Based Dissolved Oxygen Detection by Core-Shell Polymer Nanoparticles Containing Metal-Free Organic Phosphors

Youngchang Yu[+], Min Sang Kwon[+], Jaehun Jung, Yingying Zeng, Mounggon Kim, Kyeongwoon Chung, Johannes Gierschner, Ji Ho Youk,* Sergey M. Borisov,* and Jinsang Kim**

Abstract: *The highly sensitive optical detection of oxygen including dissolved oxygen (DO) is of great interest in various applications. We devised a novel room-temperature-phosphorescence (RTP)-based oxygen detection platform by constructing core–shell nanoparticles with water-soluble polymethyloxazoline shells and oxygen-permeable polystyrene cores cross-linked with metal-free purely organic phosphors. The resulting nanoparticles show a very high sensitivity for DO with a limit of detection (LOD) of 60 nM and can be readily used for oxygen quantification in aqueous environments as well as the gaseous phase.*

Quantification of dissolved oxygen (DO) in the range of 1 μM and below has recently attracted considerable attention because its urgent need in numerous applications such as corrosion protection,[1] surface treatment,[2] semiconductor industry,[3] and biological research.[4] Although a few detection systems such as membrane-inlet mass spectrometry (MIMS) and purge-and-trap gas chromatography-mass spectrometry (P&T) are able to quantify at a low level, the complex, bulky, and expensive equipment is not portable and requires trained personnel for operation, limiting its applicability for convenient and easy monitoring of DO.[4]

Optical sensors have recently become a crucial tool for quantification of DO because of their advantageous characteristics such as minimal invasiveness, miniaturization capability, versatility in formats, and suitable 2D- or 3D-imaging of DO distribution.[5,6] Optical detection of DO mostly relies on phosphorescent transition metal complexes such as polypyridyl complexes of Ru^{II} and Pd^{II} and Pt^{II} porphyrins because they possess significantly long decay lifetimes, which ensure efficient energy transfer to molecular oxygen, resulting in complete quenching of phosphorescence emission at very low DO concentrations.[6] However, concerns about the high cost, unclear toxicities, and sustainability of precious metals have incited the research community to investigate novel optical DO indicators from more abundant materials.

Metal-free organic phosphors are an emerging alternative to organometallic phosphors in a wide range of applications including organic light-emitting diodes (OLEDs), bioimaging, and sensors.[7] This new class of organic emitters can be particularly useful for highly sensitive optical DO detection because of their long decay time (from millisecond to second) originating from their inefficient spin-orbit coupling (SOC) and large Stokes shifts,[8] which enables spectral separation of excitation and emission wavelengths, resulting in simple optical set-ups and low-interference measurements. However, despite their vast potential, metal-free organic phosphors have been largely unexplored as DO indicators.[9,10,11b]

Although substantial progress has been made in the field of metal-free organic phosphors since the pioneer works from the groups of Fraser,[11] Kim,[12] and Tang,[13] bright organic phosphors at room temperature are still very rare and only limited to BF_2-chelates,[9,11,14] phenylthiobenzene,[15] benzophenone,[13,16,17] fluorene,[18,19] triazine,[20] boronic ester,[21] naphthalimide,[22] sulfone,[23] bromobenzaldehyde,[12] and polyaromatic analogues.[24,25] In addition, stringent conditions of rigid hosts such as crystalline solid-state structures and

[*] Y. Yu,[+] M. S. Kwon,[+] Y. Zeng, M. Kim, J. Kim
Department of Materials Science and Engineering, University of Michigan (USA)
E-mail: jinsang@umich.edu
J. Jung, K. Chung, J. Kim
Macromolecular Science and Engineering, University of Michigan (USA)
J. Kim
Department of Chemical Engineering, Department of Biomedical Engineering, and Department of Chemistry, University of Michigan (USA)
M. S. Kwon[+]
Department of Materials Science and Engineering, Ulsan Institute of Science and Technology (UNIST) (Korea)
E-mail: kwonms@unist.ac.kr
K. Chung
Process Innovation Department, Korea Institute of Materials Science (KIMS) (Korea)
J. Gierschner
Madrid Institute for Advanced Studies—IMDEA Nanoscience (Spain)
J. H. Youk
Department of Applied Organic Materials Engineering, Inha University (Korea)
E-mail: youk@inha.ac.kr
S. M. Borisov
Institute of Analytical Chemistry and Food Chemistry, Graz University of Technology (Austria)
E-mail: sergey.borisov@tugraz.at
[+] These authors contributed equally to this work.
Supporting information, including experimental details, and the ORCID identification number(s) for the author(s) of this article can be found under: https://doi.org/10.1002/anie.201708606.

carefully chosen polymer matrices are commonly required for bright room-temperature phosphorescence (RTP). However, practical applicability of such a phosphor-doped polymer film and a phosphorescent crystal can be rather limited and, hence, development of a new versatile platform that allows achieving bright organic RTP and thus quantifying DO at significantly low concentrations for various applications is required.

Herein, we report metal-free organic phosphors crosslinked within core–shell polymer nanoparticles as a novel versatile platform for highly sensitive detection of DO, as nanoparticles have proven to be a versatile platform for various applications including DO quantification.[26] To achieve high sensitivity, for the core part of the nanoparticles we chose metal-free organic phosphors as an indicator, considering their long phosphorescence decay time, and polystyrene (PS) as a matrix because of its high oxygen permeability. Poly(2-methyl-2-oxazoline) (PMeOx) was selected as an outer shell of the nanoparticles because of its water solubility and biocompatibility, enabling the application of DO quantification in aqueous phase for a variety of applications. Most importantly, a novel metal-free organic phosphor was rationally designed to be used as a crosslinker as well as an indicator since the restriction of molecular motion near the phosphors by covalent crosslinking through a short linker will greatly enhance phosphorescence intensity, allowing for highly sensitive detection of DO (see Figure 1). Phosphorescent core–shell nanoparticles having a well-defined diameter of circa 180 nm and 320 nm were successfully prepared by reversible addition–fragmentation chain-transfer (RAFT) dispersion polymerization of a macro-RAFT agent in the presence of the newly designed metal-free organic phosphor having a crosslinking capability (see Figure 2 and the Supporting Information).[12d]

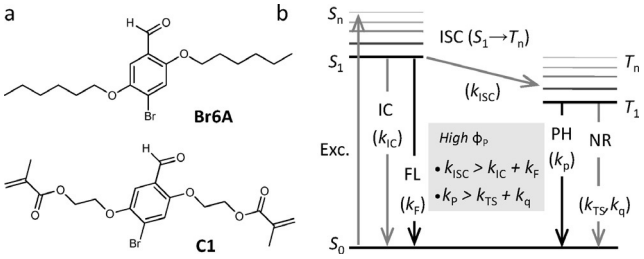

Figure 1. a) Chemical structures of the designed crosslinkable phosphor, C1, and a control, Br6A. b) A typical Jablonski diagram of organic emitters.

The realization of bright RTP from metal-free organic phosphors in a non-rigid matrix such as a polymeric nanoparticle is still a challenging issue; as far as we know, only a few examples have been reported until now.[11] Active molecular motions in a non-rigid matrix greatly promotes the radiationless decay processes such as triplet–triplet energy transfer and intersystem crossing (ISC) from T_1 to S_0, resulting in complete quenching of phosphorescence (see Figure 1b).[12,19] In fact, simple doping of a metal-free organic phosphor, Br6A, into polymeric nanoparticles showed weak phosphorescence emission even under an inert atmosphere.

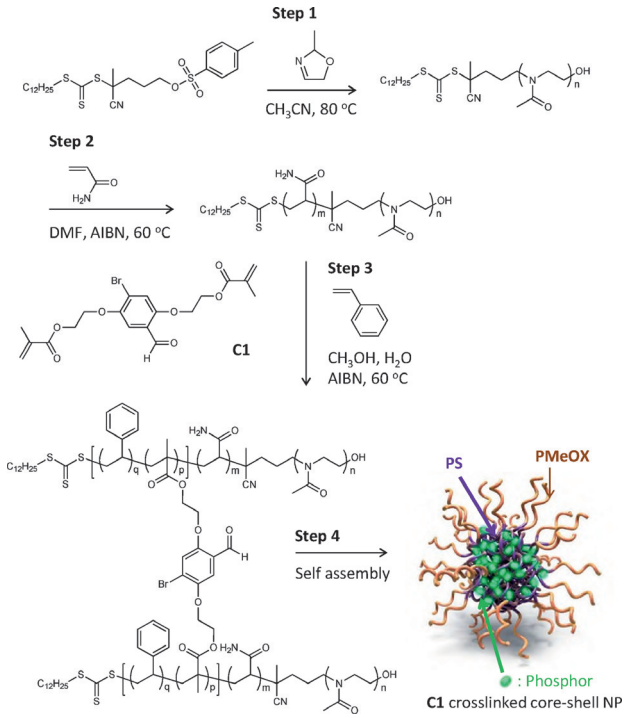

Figure 2. Synthetic routes of C1-crosslinked NPs.

To address the challenge, we introduce crosslinks between phosphors and polymers into the nanoparticle system.

The phosphor with a short saturated hydrocarbon linker (denoted as C1) was designed and synthesized as the DO indicator (see Figure 1a). To validate our molecular design, we prepared a poly(methyl methacrylate) (PMMA) having covalently crosslinked C1 and compared its phosphorescence quantum efficiency with a Br6A doped PMMA film (see the Supporting Information). As expected, C1-crosslinked PMMA showed high phosphorescence quantum efficiency of circa 40%, which is circa 3-fold higher than that of the Br6A doped film. This is attributed to the fact that a short and simple cross-linker efficiently restricts the molecular motion of phosphors as well as the polymer matrix and thereby effectively suppresses the non-radiative relaxation pathways.[12d]

We then prepared crosslinked core–shell polymeric nanoparticles based on the C1 phosphors. A macro-RAFT initiator was synthesized by using a tosyl-functionalized RAFT agent as a dual initiator in two steps.[27] Water-soluble PMeOx was first synthesized by ring opening polymerization (ROP) of methyloxazoline (MeOx) at 80°C followed by the RAFT polymerization of acrylamide (AAm) in the presence of AIBN (see Figure 2, step 1). Importantly, a PAAm block was introduced to promote the rate of RAFT polymerization of styrene[28] since the RAFT initiator is not effective for polymerization of styrene monomers (see Figure 2, step 2).[29] Once the macro-RAFT initiator was successfully prepared, the core–shell nanoparticles were then prepared through an one-pot dispersion RAFT polymerization of styrene monomers together with C1 by means of the macro-RAFT agent (see Figure 2, step 3). The resulting crosslinked amphiphilic block copolymers spontaneously self-assembled

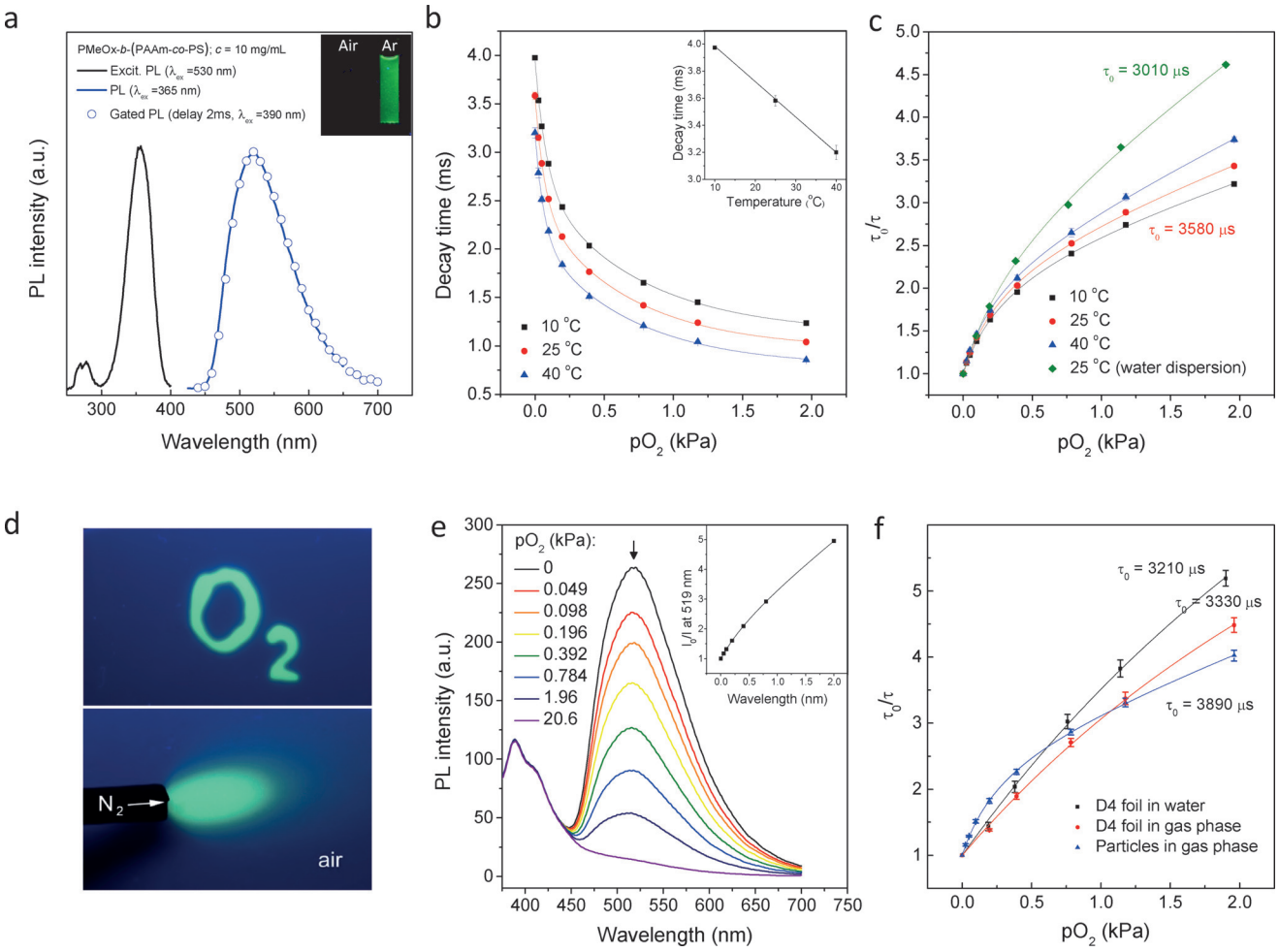

Figure 3. a) Photoluminescence (PL) emission and excitation and gated PL spectra of phosphor-crosslinked NPs dispersed in argon saturated water. The inset shows PL images of phosphor-crosslinked NPs dispersed in air-saturated (left) and argon-saturated (right) water at room temperature under a 365 nm hand-held UV light. b) Decay time plots and temperature dependency of τ_0 (inset) and c) Stern–Volmer plots of dry 180 nm beads exposure to oxygen in the gaseous phase and as aqueous dispersion (10 mg mL^{-1}, $T = 25\,°C$). d) Images obtained with an RGB camera upon illumination of the planar optical sensor with the 366 nm line of a UV-lamp. Bright green phosphorescence indicates the areas of the sensor soaked with an anoxic aqueous solution (containing 5 wt% of glucose and 0.05 wt% of glucose oxidase) for the left image and the area of the sensor deoxygenated with a flow of nitrogen (bottom image). e) Corrected luminescence spectra for the planar optode ($\lambda_{exc} = 365$ nm). Inset shows the corresponding Stern–Volmer plots ($\lambda_{max} = 519$ nm). f) Stern–Volmer plots for the sensor based on 320 nm beads dispersed in hydrogel D4 in the gas phase and in water. Response of the dry particles in the gas phase is also shown for comparison. In all the cases $T = 25\,°C$.

into well-defined functional core–shell nanoparticles (see Figure 2, step 4). The size of nanoparticle could be manipulated by controlling the amount of the macro-initiator (see the Supporting Information).

The resulting core–shell nanoparticles were characterized by scanning electron microscope (SEM), dynamic light scattering (DLS), and by emission and excitation photoluminescence (PL) spectroscopy. SEM and DLS analyses confirmed the formation of the core–shell nanoparticles with average diameters of circa 180 nm and circa 320 nm, respectively, and a narrow size distribution (see the Supporting Information, Figures S1 and S2). Figure 3a shows the PL excitation spectrum of C1-crosslinked nanoparticles, which matches well with the absorption spectrum of Br6A, clearly indicating that C1 was successfully incorporated into the nanoparticles (see the Supporting Information, Figure S3). As expected, the nanoparticles exhibited a distinct oxygen sensitivity. While the nanoparticles show essentially no phosphorescence under ambient conditions, bright phosphorescence was observed after the elimination of oxygen by nitrogen purging (see Figure 3a, inset).

The oxygen-sensing properties of the resulting nanoparticles were quantitatively analyzed in the gaseous phase first by using a phase-modulation technique. Generally, the frequency domain method allows for a compact and inexpensive instrumentation, which is important for practical applications.[30] We used a 375 nm LED for excitation, which almost perfectly matches the absorption maximum of the nanoparticles. Investigation of the dry bead agglomerates revealed a very similar behaviour for 320 and 180 nm NPs (see Figure 3b and the Supporting Information, Figure S4). As expected, nanoparticles of both sizes showed very high oxygen sensitivity, which is explained by the long phosphorescence decay time of the metal-free organic phosphor under

oxygen-free conditions ($\tau_{0,gas} \approx 4$ ms, see Figure S4). It should be mentioned that although a great number of oxygen indicators with the phosphorescence decay times from 1 to 1000 μs are available,[5,6a] there are only very few examples of probes featuring longer phosphorescence/TADF lifetimes, τ, such as C_{70} fullerene ($\tau_0 \approx 20$ ms),[9b] BF_2-chelates ($\tau_0 \approx 4.3$ ms;[11b] $\tau_0 \approx 360$–730 ms),[9a] and Gd^{III} complexes ($\tau_0 \approx 1.3$ ms; $\tau_0 \approx 2$ ms),[6e] which are of particular interest for the design of ultra-sensitive oxygen sensors. The sensitivity is slightly higher for the 320 nm NPs, which is explained by their longer decay time. To quantify the sensitivity, we measured τ as a function of oxygen pressure, pO_2, and plotted τ_0/τ as function of pO_2. The Stern–Volmer plots show a nonlinear behavior, indicating a heterogeneous environment of the quenching sites in the nanoparticles (see Figure 3c). The Stern–Volmer constants, $k_{q1,2}$, were thus evaluated by the 2-site model developed by Carraway and Demas;[31] giving 7.1 kPa^{-1} and 0.28 kPa^{-1} for the first and the second site of the 320 nm NPs, respectively; the LOD in the gas phase was estimated to be 5 Pa. Even though a linear Stern–Volmer plot is advantageous, only very few polymer-immobilized indicators show linearity[32] and a good fit with the 2-site model is fully sufficient for practical applications. The resulting high sensitivity makes our nanoparticle system promising for a wide range of industrial and environmental applications, for instance for investigation of oxygen in the oxygen minimum zones in the ocean.[33]

The nanoparticles showed some decrease in the luminescence decay time at higher temperatures (see Figure 3b and Figure S4) which is caused by thermal quenching, that is, increase of the non-radiative rate constant. The temperature coefficients are similar for both NPs and are 0.84 % K^{-1} and 0.72 % K^{-1} at 25 °C for 320 and 180 nm NPs, respectively; this is higher than those of the most common organometallic oxygen indicators such as Pt^{II} and Pd^{II} porphyrins and Ru^{II} polypyridyl complexes.[34]

Interestingly, nanoparticles dispersed in water showed more linear Stern–Volmer plots and higher sensitivity compared to those in the gas phase, despite slightly shorter decay time (see Figure 3c). The effect of humidity on the sensitivity of oxygen sensors is not uncommon for less hydrophobic polymers.[35] Therefore, the nanoparticle systems introduced in this study are excellently suitable as well for the monitoring of DO in aqueous media. The nanoparticles can be simply added to the analyte solution (for example, in concentrations of 10 mg mL^{-1}) providing that the sample volume is not too large.

In order to achieve higher flexibility in possible applications of the developed material system we prepared planar optodes by dispersing the 320 nm NPs in a polyurethane hydrogel D4. The cocktail was coated onto a transparent poly(ethylene terephthalate) (PET) substrate resulting in a thin film (about 14 μm thick) after solvent evaporation. The optodes can be used for imaging[36] of 2D oxygen distributions (illustrated by Figure 3d) or as sensor spots attached to the tip of an optical fiber or placed on the inner side of a transparent glass wall. Red-green-blue (RGB) imaging gained popularity for a variety of practical applications because of its simple and low-cost instrumentation.[37] Our nanoparticle system is highly promising for this purpose because the phosphorescence color (λ_{max} at 519 nm) matches almost perfectly the green channel of the camera (see Figure 3e). Although the blue fluorescence at circa 390 nm, originating from the PET support, is not affected by oxygen and, in principle, can be used for referencing of phosphorescence intensity, such measurement is not desirable because of interferences and large scattering effects. For that reason, a reference material which emits in the red part of the spectrum could be added to the sensor layer along with the oxygen-sensitive particles to enable ratiometric readout. Such a ratiometric system is currently under development in our labs. The Stern–Volmer plots for the planar optodes are more linear compared to that of the dry nanoparticle agglomerates (see Figure 3f). The results obtained from the steady-state emission spectra (see Figure 3e, inset) and from intensity measurements in frequency domain are very similar (see Figure 3f). The sensitivity is again somewhat higher when the measurements are performed in water compared to those with the dry optode, that is, in the gas phase.[38]

In summary, we have developed metal-free organic phosphors crosslinked within core–shell polymer nanoparticles as a novel versatile platform for highly sensitive detection of DO in a variety of water environments and gaseous oxygen. We believe that this new detection platform will be widely utilized for the convenient and easy monitoring of DO.

Acknowledgements

This work was financially supported by National Science Foundation (DMREF DMR 1435965). The work in Ulsan was supported by the 2016 Research Fund (1.160022.01) of the Ulsan National Institute of Science and Technology (UNIST) and by the Basic Science Research Program through the National Research Foundation of Korea (NRF), which was funded by the Ministry of Education (NRF-2016R1D1A1B03936002). The work at IMDEA was supported by the Spanish Ministerio de Economía y Competitividad (grant no. CTQ2014-58801).

Conflict of interest

The authors declare no conflict of interest.

Keywords: crosslinking · dissolved oxygen · metal-free organic phosphors · polymer nanoparticles · room-temperature phosphorescence

How to cite: *Angew. Chem. Int. Ed.* **2017**, *56*, 16207–16211
Angew. Chem. **2017**, *129*, 16425–16429

[1] K. Tanno, *Bull. Chem. Soc. Jpn.* **1964**, *37*, 804–810.
[2] T. Nakano, K. Hoshi, S. Baba, *Vacuum* **2008**, *83*, 467–469.
[3] H. Berger, *Microelectron. Eng.* **1991**, *10*, 259–267.
[4] a) D. A. Stolper, N. P. Revsbech, D. E. Canfield, *Proc. Natl. Acad. Sci. USA* **2010**, *107*, 18755–18760; b) D. Shevela, K. Beckmann, J. Clausen, W. Junge, J. Messinger, *Proc. Natl. Acad. Sci. USA* **2011**, *108*, 3602–3607.

[5] X. Wang, O. S. Wolfbeis, *Chem. Soc. Rev.* **2014**, *43*, 3666 – 3761.
[6] a) M. Quaranta, S. M. Borisov, I. Klimant, *Bioanal. Rev.* **2012**, *4*, 115 – 157; b) R. Briñas, T. Troxler, R. M. Hochstrasser, S. A. Vinogradov, *J. Am. Chem. Soc.* **2005**, *127*, 11851 – 11862; c) J. A. Spencer, F. Ferraro, E. Roussakis, A. Klein, J. Wu, J. M. Runnels, W. Zaher, L. J. Mortensen, C. Alt, R. Turcotte, R. Yusuf, D. Cote, S. A. Vinogradov, D. T. Scadden, C. P. Lin, *Nature* **2014**, *508*, 269 – 273; d) Y. Feng, J. Cheng, L. Zhou, X. Zhou, H. Xiang, *Analyst* **2012**, *137*, 4885 – 4901; e) S. M. Borisov, R. Fischer, R. Saf, I. Klimant, *Adv. Funct. Mater.* **2014**, *24*, 6548 – 6560.
[7] For recent reviews on metal-free organic phosphors, see: a) S. Mukherjee, P. Thilagar, *Chem. Commun.* **2015**, *51*, 109988 – 111003; b) S. Xu, R. Chen, C. Zheng, W. Huang, *Adv. Mater.* **2016**, *28*, 9920 – 9940; c) M. Baroncini, G. Bergamini, P. Ceroni, *Chem. Commun.* **2017**, *53*, 2081 – 2093; d) S. Hirata, *Adv. Opt. Mater.* **2017**, *5*, 1700116.
[8] It should be noted that a certain type of RTP emitters having high structural rigidity and small singlet–triplet energy gaps, such as benzophenone analogues, exhibits rather small Stokes shift.
[9] a) P. Lehner, C. Staudinger, S. M. Borisov, I. Klimant, *Nat. Commun.* **2014**, *5*, 4460; b) S. Nagl, C. Baleizão, S. M. Borisov, I. Klimant, *Angew. Chem. Int. Ed.* **2007**, *46*, 2317 – 2319; *Angew. Chem.* **2007**, *119*, 2368 – 2371.
[10] S. Banerjee, R. T. Kuznetsova, D. B. Pankovsky, *Sens. Actuators B* **2015**, *212*, 229 – 234.
[11] a) G. Zhang, J. Chen, S. J. Payn, S. E. Kooi, J. N. Demas, C. L. Fraser, *J. Am. Chem. Soc.* **2007**, *129*, 8942 – 8943; b) G. Zhang, G. M. Palmer, M. W. Dewhirst, C. L. Fraser, *Nat. Mater.* **2009**, *8*, 747 – 751; c) G. Zhang, J. Lu, M. Sabat, C. L. Fraser, *J. Am. Chem. Soc.* **2010**, *132*, 2160 – 2162.
[12] a) O. Bolton, K. Lee, H. J. Kim, K. Y. Lin, J. Kim, *Nat. Chem.* **2011**, *3*, 205 – 210; b) D. Lee, O. Bolton, B. C. Kim, J. H. Youk, S. Takayama, J. Kim, *J. Am. Chem. Soc.* **2013**, *135*, 6325 – 6329; c) M. S. Kwon, D. Lee, S. Seo, J. Jung, J. Kim, *Angew. Chem. Int. Ed.* **2014**, *53*, 11177 – 11181; *Angew. Chem.* **2014**, *126*, 11359 – 11363; d) M. S. Kwon, Y. Yu, C. Coburn, A. W. Phillips, K. Chung, A. Shanker, J. Jung, G. Kim, K. Pipe, S. R. Forrest, J. H. Youk, J. Gierschner, J. Kim, *Nat. Commun.* **2015**, *6*, 8947; e) O. Bolton, D. Lee, J. Jung, J. Kim, *Chem. Mater.* **2014**, *26*, 6644 – 6649.
[13] a) W. Z. Yuan, X. Y. Shen, H. Zhao, J. W. Y. Lam, L. Tang, P. Lu, C. Wang, Y. Liu, Z. Wang, Q. Zheng, J. Z. Sun, Y. Ma, B. Z. Tang, *J. Phys. Chem. C* **2010**, *114*, 6090 – 6099; b) Y. Gong, G. Chen, Q. Peng, W. Z. Yuan, Y. Xie, S. Li, Y. Zhang, B. Z. Tang, *Adv. Mater.* **2015**, *27*, 6195 – 6201.
[14] M. Koch, K. Perumal, O. Blacque, J. A. Garg, R. Saiganesh, S. Kabilan, K. K. Balasubramanian, K. Venkatesan, *Angew. Chem. Int. Ed.* **2014**, *53*, 6378 – 6382; *Angew. Chem.* **2014**, *126*, 6496 – 6500.
[15] A. Fermi, G. Bergamini, M. Roy, M. Gingras, P. Ceroni, *J. Am. Chem. Soc.* **2014**, *136*, 6395 – 6400.
[16] Y. Xie, Y. Ge, Q. Peng, C. Li, Q. Li, Z. Li, *Adv. Mater.* **2017**, *29*, 1606829.
[17] Z. Yang, Z. Mao, X. Zhang, D. Ou, Y. Mu, Y. Zhang, C. Zhao, S. Liu, Z. Chi, J. Xu, Y. Wu, P. Lu, A. Lien, M. R. Bryce, *Angew. Chem. Int. Ed.* **2016**, *55*, 2181 – 2185; *Angew. Chem.* **2016**, *128*, 2221 – 2225.
[18] J. Xu, A. Takai, Y. Kobayashi, M. Takeuchi, *Chem. Commun.* **2013**, *49*, 8447 – 8449.
[19] a) S. Hirata, K. Totani, J. Zhang, T. Yamashita, H. Kaji, S. R. Marder, T. Watanabe, C. Adachi, *Adv. Funct. Mater.* **2013**, *23*, 3386 – 3397; b) R. Kabe, N. Notsuka, K. Yoshida, C. Adachi, *Adv. Mater.* **2016**, *28*, 655 – 660.
[20] a) Z. An, C. Zheng, Y. Tao, R. Chen, H. Shi, T. Chen, Z. Wang, H. Li, R. Deng, X. Liu, W. Huang, *Nat. Mater.* **2015**, *14*, 685 – 690; b) X. Zhen, Y. Tao, Z. An, P. Chen, C. Xu, R. Chen, W. Huang, K. Pu, *Adv. Mater.* **2017**, *29*, 1606665; c) S. Cai, H. Shi, J. Li, L. Gu, Y. Ni, Z. Cheng, S. Wang, W. Xiong, L. Li, Z. An, W. Huang, *Adv. Mater.* **2017**, *29*, 1701244.
[21] Y. Shoji, Y. Ikabata, Q. Wang, D. Nemoto, A. Sakamoto, N. Tanaka, J. Seino, H. Nakai, T. Fukushima, *J. Am. Chem. Soc.* **2017**, *139*, 2728 – 2733.
[22] X. Chen, C. Xu, T. Wang, C. Zhou, J. Du, Z. Wang, H. Xu, T. Xie, G. Bi, J. Jiang, X. Zhang, J. N. Demas, C. O. Trindle, Y. Luo, G. Zhang, *Angew. Chem. Int. Ed.* **2016**, *55*, 9872 – 9876; *Angew. Chem.* **2016**, *128*, 10026 – 10030.
[23] Z. Mao, Z. Yang, Y. Mu, Y. Zhang, Y. Wang, Z. Chi, C. Lo, S. Liu, A. Lien, J. Xu, *Angew. Chem. Int. Ed.* **2015**, *54*, 6270 – 6273; *Angew. Chem.* **2015**, *127*, 6368 – 6371.
[24] D. Chaudhuri, E. Sigmund, A. Meyer, L. Rock, P. Klemm, S. Lautenschlager, A. Schmid, S. R. Yost, T. V. Voorhis, S. Bange, S. Hoger, J. M. Lupton, *Angew. Chem. Int. Ed.* **2013**, *52*, 13449 – 13452; *Angew. Chem.* **2013**, *125*, 13691 – 13694.
[25] S. Reineke, M. A. Baldo, *Sci. Rep.* **2014**, *4*, 3797.
[26] R. A. Petros, J. M. DeSimone, *Nat. Rev. Drug Discovery* **2010**, *9*, 615 – 627.
[27] Y. C. Yu, H. S. Cho, W. Yu, J. H. Youk, *Polymer* **2014**, *55*, 5986 – 5990.
[28] X. Zhang, S. Boisse, W. Zhang, P. Beaunier, F. D'Agosto, J. Rieger, B. Charleux, *Macromolecules* **2011**, *44*, 4149 – 4158.
[29] Without incorporation of the PAAm block, RAFT polymerization of styrene was not successful because of a few possible problems such as low conversion, homopolymer formation, and broad size distribution of nanoparticles.
[30] O. S. Wolfbeis, *BioEssays* **2015**, *37*, 921 – 928.
[31] E. R. Carraway, J. N. Demas, B. A. DeGraff, J. R. Bacon, *Anal. Chem.* **1991**, *63*, 337 – 342.
[32] S. M. Borisov, P. Lehner, I. Klimant, *Anal. Chim. Acta* **2011**, *690*, 108 – 115.
[33] N. Revsbech, L. H. Larsen, J. Gundersen, T. Dalsgaard, O. Ulloa, *Limnol. Oceanogr. Methods* **2009**, *7*, 371 – 381.
[34] S. M. Borisov, I. Klimant, *Anal. Chem.* **2007**, *79*, 7501 – 7509.
[35] K. Eaton, P. Douglas, *Sens. Actuators B* **2002**, *82*, 94 – 104.
[36] M. Schäferling, *Angew. Chem. Int. Ed.* **2012**, *51*, 3532 – 3554; *Angew. Chem.* **2012**, *124*, 3590 – 3614.
[37] a) M. Larsen, S. M. Borisov, B. Grunwald, I. Klimant, R. N. Guld, *Limnol. Oceanogr. Methods* **2011**, *9*, 348 – 360; b) X. Wang, R. J. Meier, M. Link, O. S. Wolfbeis, *Angew. Chem. Int. Ed.* **2010**, *49*, 4907 – 4909; *Angew. Chem.* **2010**, *122*, 5027 – 5029; c) R. J. Meier, L. H. Fischer, O. S. Wolfbeis, M. Schaferling, *Sens. Actuators B* **2013**, *177*, 500 – 506.
[38] The photostability of our optical sensor system is discussed in detail in the Supporting Information.

Manuscript received: August 21, 2017
Revised manuscript received: September 27, 2017
Accepted manuscript online: November 6, 2017
Version of record online: November 22, 2017

